Advanced Steel Construction – Vol. 20 No. 2 (2024) 188–198
DOI:10.18057/IJASC.2024.20.2.11
(Special Issue: *11st International Conference on Advances in Steel Structures, ICASS'2023, Kuching, Sarawak, Malaysia*)

TESTS, MODELLING AND DESIGN OF UNSYMMETRICAL BACK-TO-BACK COLD-FORMED STEEL ANGLES UNDER COMPRESSION

Beulah Gnana Ananthi. G [1, *], Kushal Ghosh [2], Krishanu Roy [2, *], Asraf Uzzaman [3] and James B.P. Lim [2]

[1] *Department of Civil Engineering, College of Engineering Guindy campus, Anna University, Chennai 600025, India*
[2] *School of Engineering, The University of Waikato, Hamilton 3216, New Zealand*
[3] *University of the West of Scotland, United Kingdom*
** (Corresponding author: E-mail: beulah28@annauniv.edu, kris.roy@waikato.ac.nz)*

ABSTRACT

Built-up cold-formed steel (CFS) unsymmetrical angles are increasingly used in structures such as portal frames, roof trusses, and transmission towers. However, there are limited studies on CFS unequal back-to-back angle columns (BBUAC) with stiffeners. This paper presents the results of six experimental tests on intermediate BBUAC with intermittent screw fasteners. The findings include the deformed shapes at failure and the load-axial shortening behavior. Additionally, a nonlinear finite element (FE) model that accounts for both material and geometric nonlinearity was developed. The experimental results were used to validate this FE model. The paper presents a total of 166 new data points, which include six concentric compressive tests and 160 finite element analysis (FEA) results on the compressive strength of BBUAC. The effectiveness of the current design rules, based on the Direct Strength Method (DSM), was also evaluated. The evaluation revealed that the current DSM is unconservative. As a result, a modified DSM approach is proposed.

ARTICLE HISTORY

Received: 22 May 2024
Revised: 15 June 2024
Accepted: 15 June 2024

KEYWORDS

Unsymmetrical back-to-back angles;
Cold-formed steel;
Axial capacity;
Local buckling;
Flexural buckling;
Finite element modelling

1. Introduction

Back-to-back unsymmetrical built-up cold-formed steel (CFS) angle columns (BBUAC) are commonly used in CFS construction [1–8]. To prevent independent buckling of angle sections in such composite designs, either welds or screws are applied intermittently at specified positions along their height. Both the North American Iron and Steel Institute (AISI) [9] and the Australian and New Zealand Standards (AS/NZS) [10] recommend adjusting the slenderness ratio to account for the placement of these fasteners. Recent work has explored the fusion of multiple angles (starred angles - Ananthi et al. [11]) to enhance the load-bearing capacity of these columns through composite action.

Apart from recent studies by Ananthi et al. [12-13] and Deepak et al. [14] on CFS back-to-back angle sections with intermittent stiffeners under concentric compression, little similar research exists in the literature. Notably, research on CFS compound angle sections without stiffeners under axial compression has been conducted by Vishnuvardhan et al. [15] and Qu et al. [16]. Ananthi [17] investigated the concentric compressive capacity of CFS compound box sections formed by joining two equal angles with intermittent screws. Ananthi et al. [12-13] also studied the behavior of CFS single and starred angles under concentric compression. However, besides the studies by Ananthi et al. ([2–3, 12-13]), no research has been reported on compound columns using intermittent stiffeners with both equal and unequal angles.

Back-to-back unequal angles offer a significant advantage where the longer leg can bear the load in case of local buckling failure once it reaches its yield stress limit (Ananthi et al. [12]). Additionally, Dar et al. [18], Aghoury et al. [19], and Anbarasu et al. [20] investigated the concentric compressive capacity of CFS columns with battens composed of four unlipped angles. Young and Chen [21] conducted column tests on CFS sections with uneven lipped angles, while Shi et al. [22] performed experimental and finite element evaluations on steel equal angle columns. Ellobody and Young [23] explored the fabrication of CFS single unequal angle sections as compression members.

This study experimentally investigates the concentric compressive capacity of intermediate-length BBUAC sections with and without intermittent stiffeners (see Fig. 1). Subsequently, a nonlinear finite element (FE) model incorporating geometric and material non-linearities, as well as intermittent fasteners, was developed and validated against the experimental results. Using this validated model, parametric studies were conducted on 160 FE models, varying from stub (300 mm) to slender (2000 mm) columns.

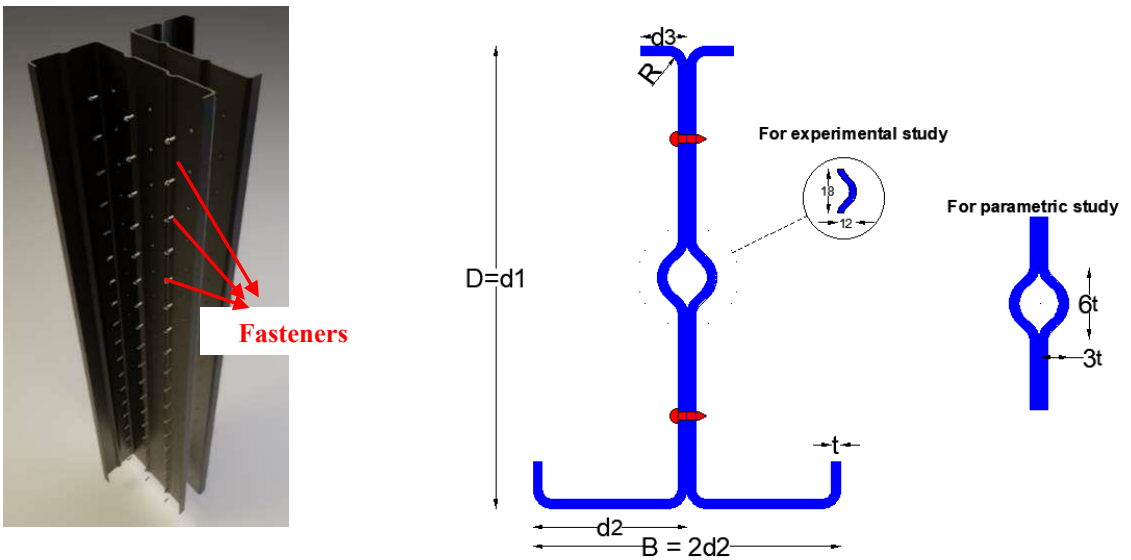

Fig. 1 Fasteners and stiffener details

To compare the experimental and FE-derived concentric compressive capacities with current design standards for stiffened BBUAC, this study presents detailed analyses and findings (see Figs. 1 and 2). The reports cover aspects such as failure modes, column length, and the effects of axial shortening under load on stiffened BBUAC. Notably, based on literature review, no existing study has analyzed the axial strength of BBUAC with various B/D ratios, which is addressed analytically in this study.

The experimental and parametric investigation results were further utilized to predict the concentric compressive strengths of BBUAC and assess their strengths in accordance with the Direct Strength Method (DSM) guidelines. An improved design equation for BBUAC is proposed based on experimental and FE findings, aiming to enhance the reliability of predicting the concentric compressive strengths of BBUAC sections with intermittent stiffeners.

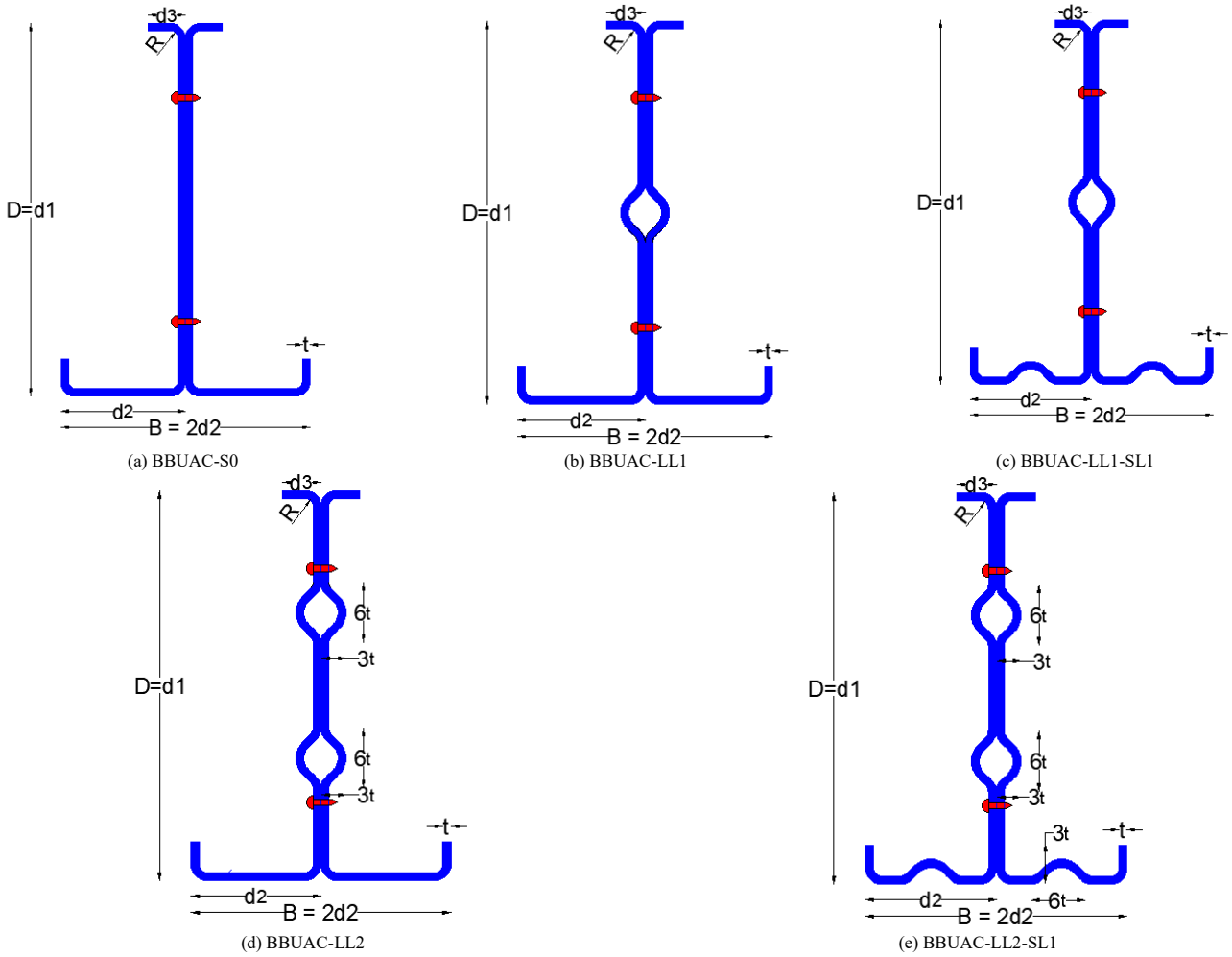

(a) BBUAC-S0 (b) BBUAC-LL1 (c) BBUAC-LL1-SL1

(d) BBUAC-LL2 (e) BBUAC-LL2-SL1

Fig. 2 Details of BBUAC examined in the experimental and parametric studies

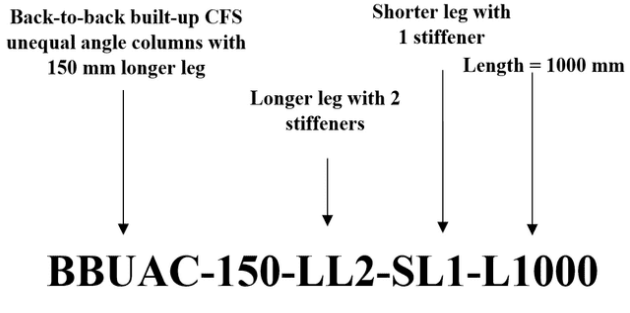

Fig. 3 BBUAC labelling

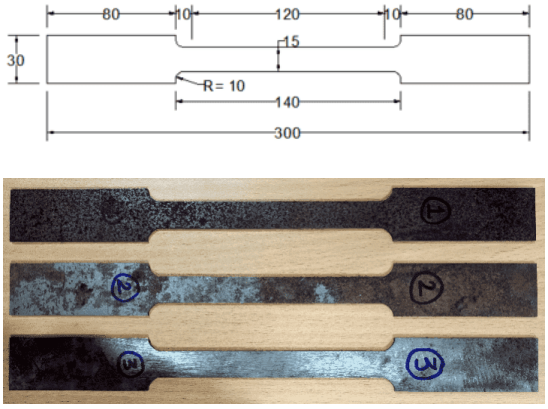

Fig. 4 Specification of coupons (cut from segments after forming)

2. Experimental investigation

2.1. Test specimen details

The experimental program focused on BBUAC configurations as depicted in Fig. 1. These consisted of two unequal angles joined to form unsymmetrical back-to-back angles using intermediate fasteners spaced 50 mm apart (refer to Fig. 1). The screw spacing was chosen in accordance with AISI [9] specifications for CFS built-up columns. Fig. 2 illustrates the B/D ratios considered: 0.75 and 1 for BBUAC120, and 0.67 and 1.00 for BBUAC150. Table 1 presents the new experimental results for six intermediate BBUAC sections.

2.2. Section labels

Labels assigned to the built-up sections denote angle section geometry, section type, and placement of intermittent stiffeners. Fig. 3 shows the labelling used in both the test program and parametric studies. For instance, BBUAC150-LL2-SL1-L300, explained as follows:

- **BBUAC150**: Unsymmetrical back-to-back angles formed using 2 unsymmetrical angles with a longer leg of 150 mm.
- **LL2**: Longer leg with 2 intermittent stiffeners.
- **SL1**: Shorter leg with 1 intermittent stiffener.
- **L300**: Column length of 300 mm.

2.3. Material testing

To characterize the material properties of the test specimens, tensile coupon tests were conducted following EN standards ISO 6892-1-2009 [24] (see Fig. 4). Testing was performed using the Zwick/Roell Z100 kN electromechanical testing equipment, as depicted in Fig. 5. The coupons underwent a loading applied at a constant crosshead speed of 0.01 mm/s. Fig. 6 presents stress-strain curves for the tested steel, including modulus of elasticity, yield stress, and ultimate stress values.

Fig. 5 Electromechanical testing machine (Zwick/Roell Z100 kN)

Table 1
FEA results against experimental results for BBUAC intermediate length sections

BBUAC: ID							Experimental results	FEA results		Design strengths (DSM)		
L=1000mm- S=50	d_1(mm)	d_2(mm)	d_3(mm)	T (mm)	L(mm)	S(mm)	P_{EXP} (kN)	P_{FEA} (kN)	P_{EXP} / P_{FEA}	P_{DSM} (kN)	P_{EXP}/ P_{DSM}	Buckling pattern
I: No stiffeners												
BBUAC120-S0-L1000	120.00	60.00	15.00	2.00	1000	50.00	102.03	108.55	0.94	89.99	1.13	Local+Flexural
BBUAC150-S0-L1000	150.00	75.00	15.00	2.00	1000	50.00	130.24	127.86	1.02	97.23	1.34	Local+Flexural
II: Longer leg with one stiffener												
BBUAC120-LL1-L1000	120.00	60.00	15.00	2.00	1000	50.00	141.38	138.60	1.02	95.73	1.48	Local+Flexural
BBUAC150-LL1-L1000	150.00	75.00	15.00	2.00	1000	50.00	138.35	142.07	0.97	105.59	1.31	Local+Flexural
III: Longer leg with two stiffener												
BBUAC150-LL2-L1000	150.00	75.00	15.00	2.00	1000	50.00	155.25	152.80	1.02	109.12	1.42	Local+Flexural
IV: Longer leg with two stiffener and one stiffener in the shorter leg												
BBUAC150-LL2-SL1-L1000	150.00	75.00	15.00	2.00	1000	50.00	158.83	161.34	0.98	123.06	1.29	Local+Flexural
Mean	-	-	-	-	-	-	-	-	**0.99**	-	**1.33**	-
COV	-	-	-	-	-	-	-	-	**0.03**	-	**0.09**	-

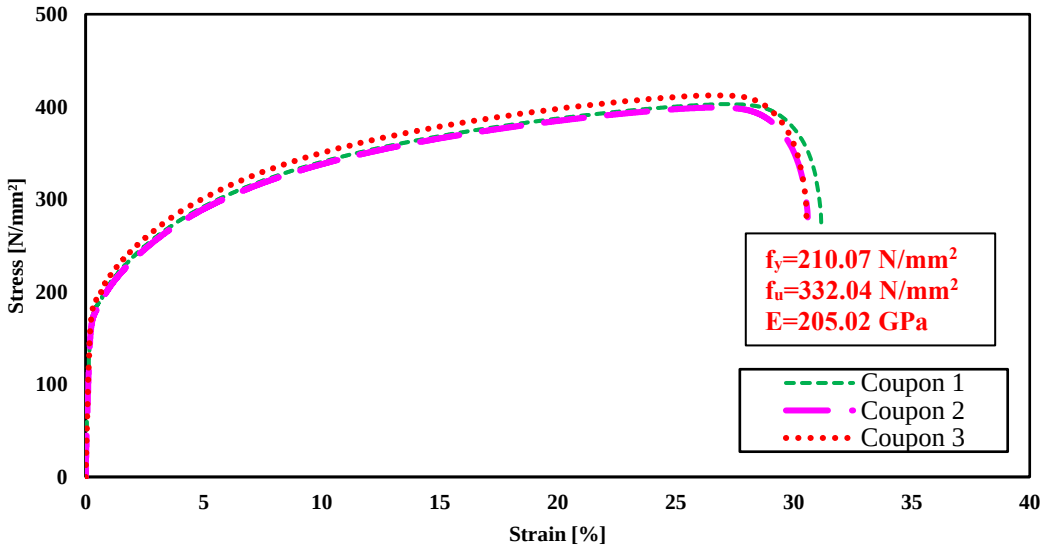

Fig. 6 Full stress-strain curve of BBUAC used in this research

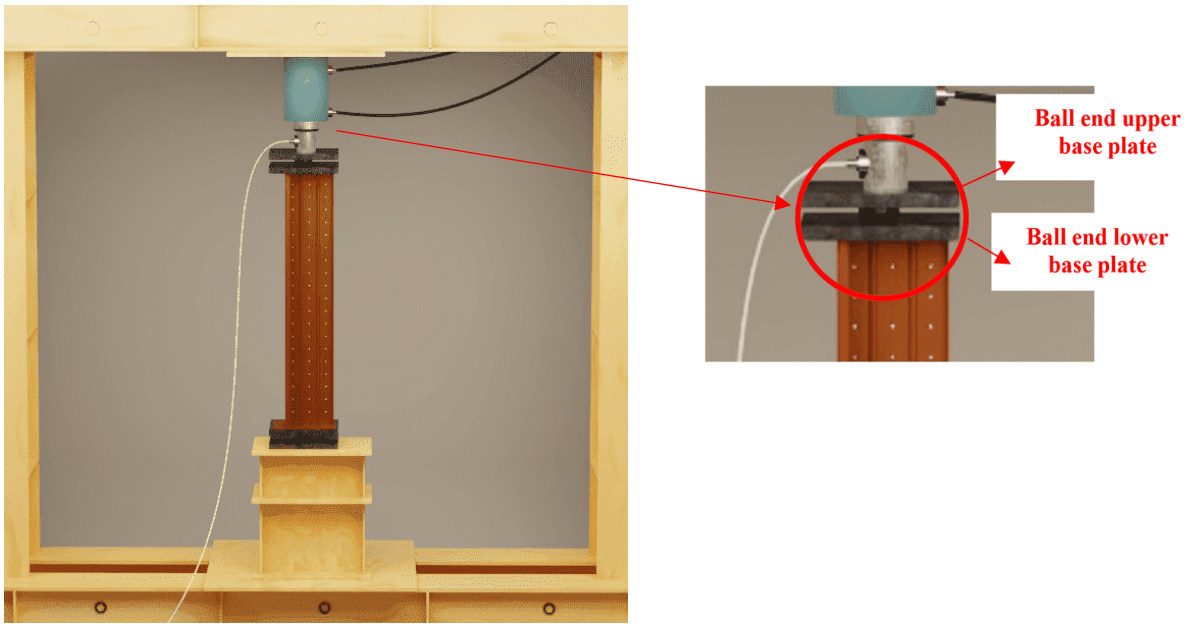

Fig. 7 Details of the experimental test

2.4. Experimental setup and loading techniques

The tests were conducted using a 100-tonne capacity loading frame, with a hydraulic ram and pump equipped with a 50-tonne capacity load cell for applying the load. The experimental specimens were supported under pinned boundary conditions at both ends, where two 200 mm x 200 mm x 10 mm thick end plates were welded to the specimen ends. To facilitate axial loading, a spherical groove measuring 150 mm x 150 mm and 25 mm thick was positioned between these plates. Additionally, a 40 mm spherical ball was placed within the groove to prevent the section from rotating or twisting around its longitudinal axis.

A machined base plate provided a level surface at the top and was welded to support the weight of the sections, ensuring the center of gravity aligned with the loading point. Fig. 7 illustrates the configuration of the test setup. Axial loading on the columns was applied using displacement control technique, with increments set to 1/10th of the maximum load and a loading rate of 0.35 mm/min. Beyond the maximum load, readings were taken to assess buckling strength until failure for each column specimen.

2.5. Test results

Table 1 presents six new experimental findings for the intermediate BBUAC specimens, complementing the concentric compressive strengths (P_{EXP}) reported by Ananthi et al. [12] for stub and short columns. Notably, BBUAC sections with two stiffeners in the longer leg and one stiffener in the shorter leg exhibit an average 16% higher concentric compressive strength compared to sections with only two stiffeners in the longer leg, as detailed in Table 1.

Fig. 8 illustrates the correlation between load and axial shortening for BBUAC150 intermediate-length columns. It shows a primarily linear relationship for BBUAC150-LL1-L1000, BBUAC150-LL2-L1000, and BBUAC150-LL2-SL1-L1000 up to 87%, 91%, and 96% of their respective ultimate failure loads (120 kN, 140 kN, and 152 kN). Non-linear behaviour is observed beyond the failure load.

Fig. 9 provides typical images depicting the failure modes of BBUAC150-S0-L1000, BBUAC150-LL1-L1000, BBUAC150-LL2-L1000, and BBUAC150-LL2-SL1-L1000 specimens from the experiments.

The concentric compressive strengths for sections with multiple stiffeners in the vertical leg with a greater B/D ratio were found to be much better than those for sections with only one longer leg stiffener. For intermediate columns, additional stiffener in the vertical leg improved the built-up sections' strength by an additional 10% on average. Only 15% of the additional strength was attributed to the shorter leg of the intermediate BBUAC's longitudinal stiffener, but it significantly contributed reducing the inside deflection along the major axis of the horizontal legs.

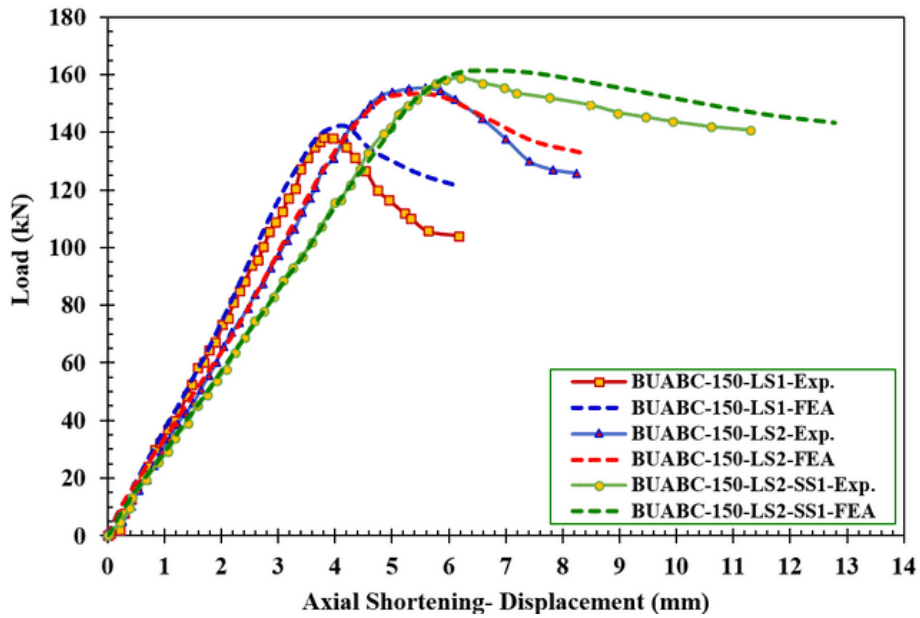

Fig. 8 Load versus axial shortening-displacement graphs for BBUAC

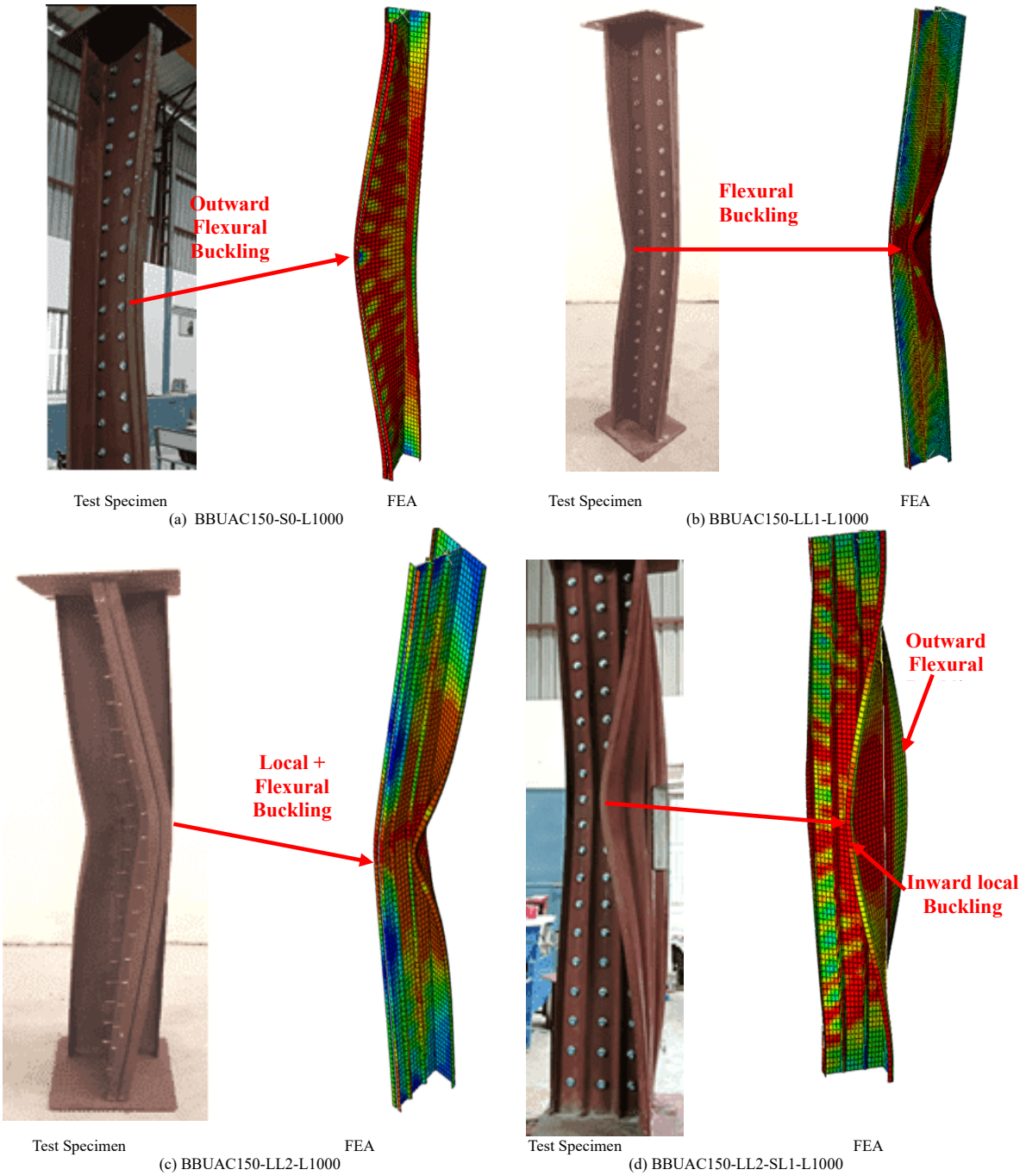

Fig. 9 Failure shapes for BBUAC for 1000 mm length

3. Finite element modelling

3.1. General

Finite Element (FE) models of the BBUAC sections subjected to axial compression were created using ABAQUS software version 6.18 [25]. Initially, linear buckling modes of the BBUAC were identified through eigenvalue analysis (BUCKLE), a feature available in the ABAQUS library. Subsequently, a non-linear analysis was performed using the Riks method. These FE models incorporated both local and global geometric imperfections, as well as material non-linearity. Detailed methods for these models are discussed in the following sections.

3.2. Geometrical and Material Properties

The study modelled the entire BBUAC geometry interconnected by fasteners. A metal plasticity model was applied for analysis and verification. In Section 5, which covers the parametric study, a simplified stress-strain curve adhering to the Von Mises yield criterion for elastic-perfect plastic behaviour was used. Stress and strain curves (engineering) obtained from coupon tests were converted into true stress and strain data for integration into the FE models (as per the equations below)

$$\sigma_{true} = \sigma(1+\varepsilon) \quad (1)$$

$$\varepsilon_{true} = \ln(1+\varepsilon) - {}^{\sigma_{true}}/_{E} \quad (2)$$

3.3. Contact surface and fastener modelling

The interaction between the longer legs of BBUAC sections was modelled using surface-to-surface contact (Fig. 10(a)). Normal contact was defined as "hard," assuming no penetration between the BBUAC sections. Since friction between parts was negligible, a frictionless interaction property was specified in the tangential direction, allowing surfaces to slide freely past each other [20].

There were no indications of fastener failures such as pulling, shearing, or tipping in Section 2.5, suggesting that the stiffness of the fasteners prevented sliding between overlapping sections of BBUAC. Self-tapping screws were used as fasteners to join the two unequal angles, with or without stiffeners, forming the BBUAC sections.

Fasteners were modelled using "beam elements" as point-based connections (Fig. 10(b) and (c)). Similar techniques can be found in the work of Ananthi et al. [20]. The fasteners were modelled with stiff surfaces and contact interactions, ensuring they did not experience shear failure (Fig. 10(d)).

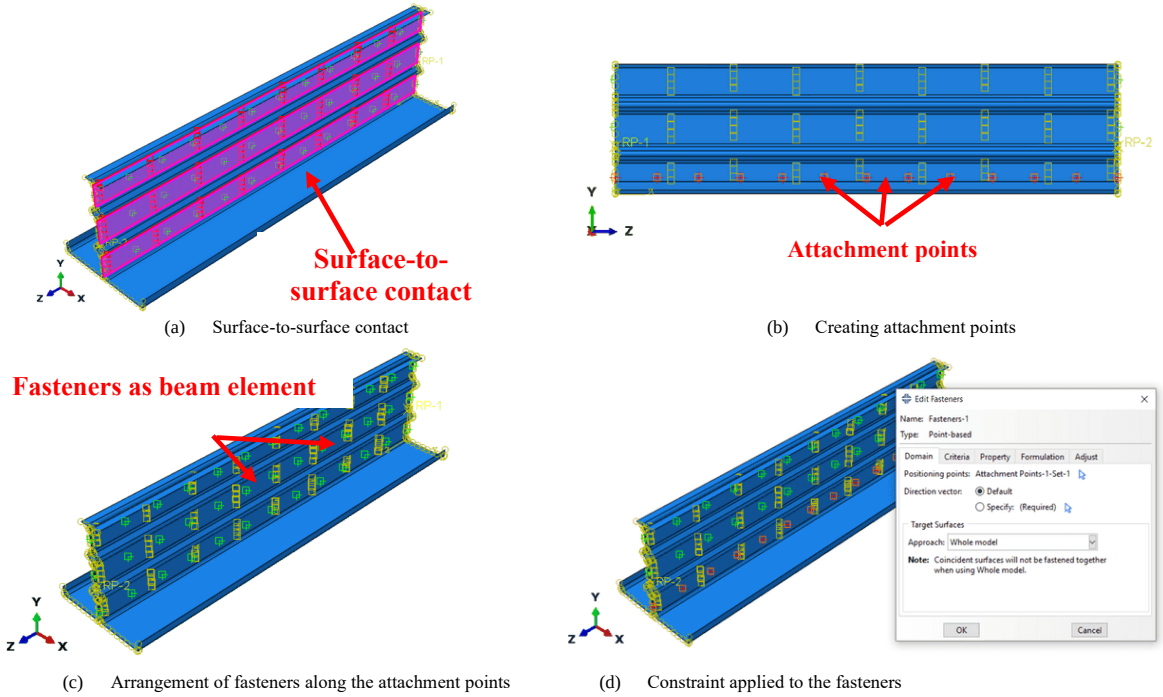

(a) Surface-to-surface contact (b) Creating attachment points

(c) Arrangement of fasteners along the attachment points (d) Constraint applied to the fasteners

Fig. 10 Contact surface and fasteners modelling for BBUAC150-LL2-L600

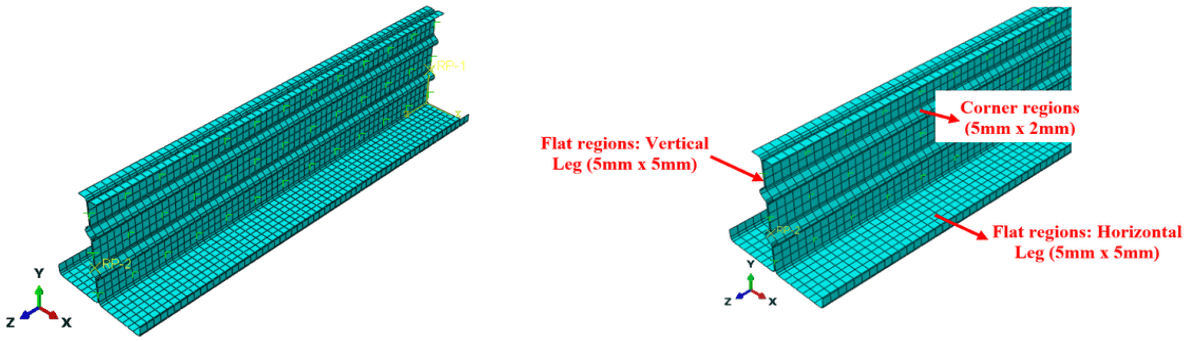

Fig. 11 FE meshing for BBUAC150-LL2-L600

A crucial factor in the structural performance of compound CFS sections is that of shear deformation. However, in this study, shearing, pulling, or tilting failure did not occur with the fasteners connecting the legs of BBUAC, as illustrated in Fig. 9. Additionally, there was no shear failure in the longer legs-connected fasteners, which kept the fasteners from moving. It should be noted that the end plates showed no signs of plate curling or cracking. It should be noted that the end plates showed no signs of plate curling or cracking.

3.4. Element type and FE meshing

The BBUAC sections (S0, LL1, LL2, LL1-SL1, and LL2-SL1) were modelled using 4-noded S4R5 quadrilateral thick shell elements, offering five degrees of freedom (DOFs) per node. This element type accommodates large rotations but assumes constant thickness throughout deformation and negligible strains.

Following a mesh sensitivity analysis, a mesh size of 5 mm × 5 mm was determined suitable for the dimensions of BBUAC sections. Aspect ratios close to 1 were maintained across BBUAC sections by adjusting the number of elements. Sample mesh patterns for the BBUAC150-LL2-L600 section are illustrated in Fig. 11. Similar modelling technique was used by Ananthi et al. [26], Fang et al. [27–28], Roy et al. [29-30], Dai et al. [31], Chen et al. [32], Masood et al. [33], and Liang et al. [34] for CFS columns.

3.5. Boundary and loading conditions

The FE model used simply supported end conditions with free edges. Translations were represented by U1, U2, and U3, and rotations in the x, y, and z directions by UR1, UR2, and UR3, respectively. Reference points RP1 and RP2, coinciding with the centres of gravity (CG) at both ends of BBUAC sections, were tied to all node sets using rigid body tie constraints (Fig. 12(a)).

An axial load was applied at the top end of RP2, with load distributed evenly along edges connected to RP (Fig. 12(b)). At RP2, major load was applied after releasing axial DOF and minor axis rotation (Fig. 12(c)), while all DOFs at RP1 were constrained except minor axis rotation (Fig. 12(d)). This setup simulated realistic experimental boundary conditions, ensuring no eccentricity in loading due to alignment of vertical centroidal axis and load line.

3.6. Modelling of initial geometric imperfections

Fabrication processes introduce initial imperfections in compression members affecting local and global buckling behaviour. Both local and global imperfections were considered, by performing eigenvalue analysis of BBUAC sections with varying thicknesses. Global and local imperfections were defined as 1/1000 times the column length and 0.006 times the thickness (wt) at mid-height, respectively, following Schafer and Pekoz [35]. First global and third local buckling modes are shown in Fig. 13 for BBUAC150-LL2-L600, derived from FEA. No distortional buckling occurred in any of the BBUAC specimens studied.

3.7. Validation of the FE model

Ultimate axial capacities from FEA (P_{FEA}) were compared with experimental capacities (P_{EXP}) for 1000 mm column lengths (Table 1). The average P_{EXP}/P_{FEA} ratio was 0.99 with a coefficient of variation (COV) of 0.03, indicating good agreement between tests and FEA results. Fig. 8 demonstrates the correlation between P_{EXP} and P_{FEA} load-axial shortening behaviour for BBUAC150 intermediate columns, showing consistent results across different configurations (Fig. 9).

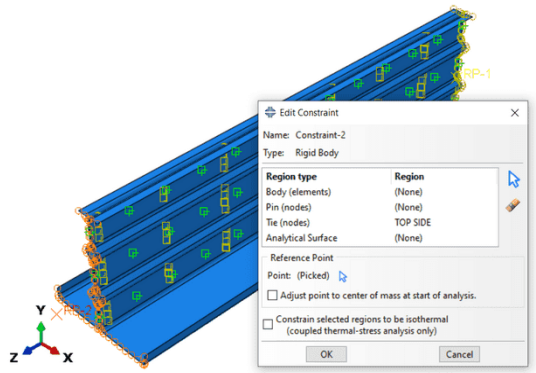

(a) Merging all nodes at the ends using rigid body constraint

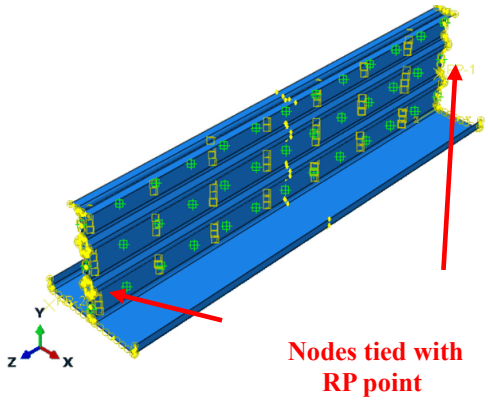

(b) Edges are tied to the reference points

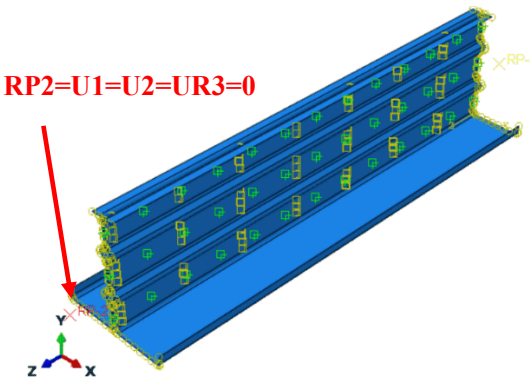

(c) Upper reference point with restraint conditions

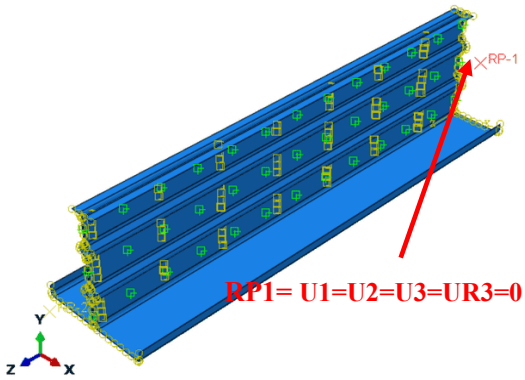

(d) Lower reference point with restraint conditions

Fig. 12 Applied boundary condition for BBUAC150-LL2-L600

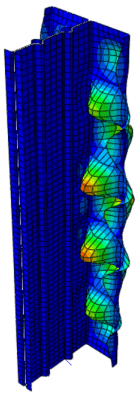

(a) Local buckling

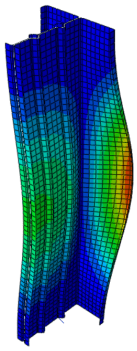

(b) Global buckling

Fig. 13 Initial imperfection contours for BBUAC150-LL2-L600, obtained from the FEA

4. Design guidelines as per AISI [9] and AS/NZ [10] standards

The unfactored axial capacity of BBUAC sections can be calculated using the guidelines provided by the AISI [9] and AS/NZS [10] design standards. The design capacity of these BBUAC sections can be determined in compliance with the given design requirements by utilising the effective width method (EWM) and DSM methodology.

$$P_{AISI\&AS/NZS} = A_e F_n \tag{3}$$

The critical buckling stress (F_n) can be calculated using Equations 4 and 5 as follows:

$$\text{For } \lambda_c \leq 1.5, F_n = \left(0.658^{\lambda^2}\right) F_y \tag{4}$$

$$\text{For } \lambda_c > 1.5, F_n = \left(\frac{0.877}{\lambda_c^2}\right) F_y \tag{5}$$

The non-dimensional critical slenderness (λ_c) can be calculated using Equation 6 as given below:

$$\lambda_c = \sqrt{\frac{F_y}{F_e}} \tag{6}$$

The minimal value of the local buckling capacity (P_{nl})), distortional buckling capacity (P_{nd}), and global buckling capacity (P_{ne}) is used to calculate the design capacity (P_{DSM}) for BBUAC sections [Equation 7].

$$P_{DSM} = \min\left(P_{ne}, P_{nl}, P_{nd}\right) \tag{7}$$

Eqs. (8–10) provide the design equations to determine the local buckling capacity (P_{nl}):

$$For\ \lambda_l \leq 0.776\ ; P_{nl} = P_{ne} \tag{8}$$

$$For\ \lambda_l > 0.776\ ; P_{nl} = \left[1 - 0.15\left(\frac{P_{crl}}{P_{ne}}\right)^{0.4}\right]\left(\frac{P_{crl}}{P_{ne}}\right)^{0.4} P_{ne} \tag{9}$$

$$\lambda_l = \sqrt{\frac{P_{ne}}{P_{crl}}} \tag{10}$$

Eqs. (11–13) provide the design equations to determine the distortional buckling capacity (P_{nd}):

$$For\ \lambda_d \leq 0.561\ ; P_{nd} = P_y \tag{11}$$

$$For\ \lambda_d > 0.561\ ; P_{nd} = \left[1 - 0.25\left(\frac{P_{crd}}{P_y}\right)^{0.6}\right]\left(\frac{P_{crd}}{P_y}\right)^{0.6} P_y \tag{12}$$

$$\lambda_d = \sqrt{\frac{P_y}{P_{crd}}} \tag{13}$$

Eqs. (14–16) provide the design equations to determine the global buckling capacity (P_{ne}):

$$For\ \lambda_c \leq 1.5\ ; P_{ne} = \left(0.658^{\lambda_c{}^2}\right) P_y \tag{14}$$

$$For\ \lambda_c > 1.5\ ; P_{ne} = \left(\frac{0.877}{\lambda_c{}^2}\right) P_y \tag{15}$$

$$\lambda_c = \sqrt{\frac{P_y}{P_{cre}}} \tag{16}$$

The nominal design concentric compressive strength of BBUAC sections was calculated using the aforementioned equations both with and without stiffeners. The joinery details between the two angle sections were replicated in this analytical model by imposing strict constraints at the locations of fasteners, such as in the x, y, and z directions, with degrees of freedom being controlled. The longitudinal degrees of freedom (in the y direction) were unrestricted along the length. In Tables 1 for the intermediate BBUAC with and without stiffeners, the design concentric compressive strengths estimated by the DSM equations are contrasted with the experimental and FE values.

5. Parametric study

A comprehensive parametric study was conducted using a validated FE model to evaluate the adequacy of current Direct Strength Method (DSM) guidelines. This study focused on the geometrical configurations of built-up unequal angles previously examined (BBUAC 120 and BBUAC 150) by Ananthi et al. [12]. Five distinct geometries (BBUAC-S0, BBUAC-LL1, BBUAC-LL1-SL1, BBUAC-LL2, and BBUAC-LL2-SL1) were investigated, varying between longer leg dimensions of 120 mm and 150 mm, and lengths ranging from 300 mm to 2000 mm.

Key findings from the parametric analysis include:

- BBUAC150-LL2 sections with two intermittent stiffeners in the longer leg and a B/D ratio greater than 0.67 exhibited superior concentric compressive strengths compared to sections with only a single intermittent longitudinal stiffener.
- Axial strength for BBUAC120-LL1 specimens with B/D ratios of 0.75 and 1.00 increased by approximately 5% compared to specimens from the BBUAC120-S0 series, irrespective of section thickness.
- While the addition of a shorter intermittent stiffener effectively controlled inward buckling along the major axis, it did not significantly enhance the axial strength. The multiple stiffeners reduced plate slenderness, contributing to increased axial strength.
- Failure mode analyses using the validated FE model indicated significant strength reduction beyond 1000 mm for all columns, regardless of thickness.
- Fig. 14 illustrates the failure modes of BBUAC150-LL1 (B/D: 1.00) series columns at different lengths (300 mm, 600 mm, 1000 mm, 1500 mm, and 2000 mm), showing evident signs of local and flexural buckling in columns longer than 1000 mm. Shorter columns (stub and short) with a thickness of 2 mm failed primarily due to local buckling.

Observations from the parametric study further revealed:

- Longitudinal intermittent stiffeners increase the nominal area of the plate and improve its buckling resistance. A single longitudinal stiffener can delay flexural buckling after local buckling but has limited impact on the load-carrying capacity.
- Fastener spacing used in this study was found adequate as no local buckling occurred between fastener spacings for both BBUAC120 and BBUAC150 configurations.
- Stiffeners effectively prevented out-of-plane local buckling in BBUAC150 sections, as evidenced by comparison of buckling modes.
- Failure in all intermediate and slender columns of both BBUAC120 and BBUAC150 was consistently attributed to combined local and flexural buckling, regardless of slenderness ratio or dimension ratio.
- Despite changes in B/D ratios from 0.67/0.75 to 1.00, the failure pattern remained consistent.

The study concluded that the number of fasteners specified in AISI S100-2016 [9] standard is sufficient to maintain the integrity of BBUAC sections, even for thinner columns, as no fasteners failed simultaneously during the analyses. These findings provide valuable insights into optimizing the design and performance of CFS compound unequal angle section columns under different loading conditions.

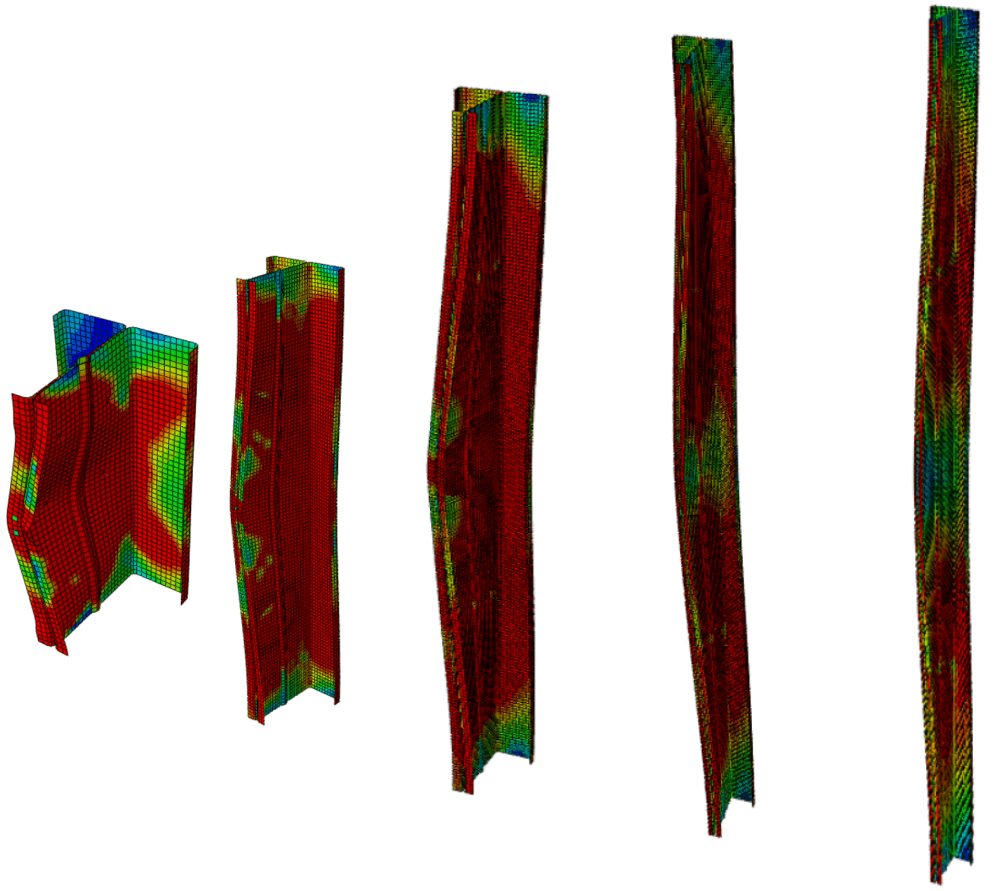

(i) L=300 mm (ii) L=600mm (iii) L=1000 mm (iv) L=1500mm (v) L=2000 mm

Fig. 14 Deformed shapes at failure for BBUAC150-LL1 (B/D:1.00) for 3 mm thickness from the FEA

6. Proposed design equations

The design curves outlined in AISI S100-2016 [9] and AS/NZS 4600:2018 [10] are typically categorized into two main regions. As detailed in Section 4 of this study, the first region applies when $\lambda_c \leq 1.5$ for flexural buckling, while the second region pertains to $\lambda_c > 1.5$. Similarly, for local buckling modes, the first region is defined when $\lambda_l \leq 0.776$, with the second region applicable when $\lambda_l > 0.776$.

Both AISI S100-2016 [9] and AS/NZS 4600:2018 [10] have been found to be overly conservative in estimating the axial strength of BBUAC, prompting this study to propose modifications to current design guidelines for determining BBUAC's concentric compressive strengths. Equations 12 and 13 introduce a modified column curve recommended by this study, aimed at providing safer, more accurate, and less scattered strength estimates. The new column curve is formulated as follows:

The concentric compressive flexural buckling strengths ($P_{Proposed\text{-}1}$) is given by Equation 17.

$$P_{Proposed-1}\begin{cases}\left(0.95^{\lambda^{1.35}_c}\right)P_y & \text{for } \lambda_c < 1.0\\ \left(\frac{1.45}{\lambda^{1.45}_c}\right)P_y & \text{for } \lambda_c \leq 1.7\\ \left(\frac{1.25}{\lambda^{1.15}_c}\right)P_y & \text{for } \lambda_c > 1.7\end{cases} \quad (17)$$

The concentric compressive local buckling strengths ($P_{Proposed-2}$) is given by Equation 18.

$$P_{Proposed-2}=\begin{cases}P_{ne} & \text{for } \lambda_l \leq 0.776\\ 1.25\left[1-0.15\left(\frac{P_{crl}}{P_{ne}}\right)^{0.4}\right]\left(\frac{P_{crl}}{P_{ne}}\right)^{0.4}P_{ne} & \text{for } \lambda_l > 0.776\end{cases} \quad (18)$$

Where

- P_{crl} is the elastic buckling load
- P_{crd} is the distortional buckling load
- P_{cre} is the global buckling load

These equations aim to better predict the concentric compressive strengths of BBUAC sections, taking into account both local and flexural buckling behaviours observed in the experimental and numerical studies conducted in this research. The proposed design strengths ($P_{Proposed\text{-}1}$ and $P_{Proposed\text{-}2}$) and the FEA coincide quite closely, as seen in Figs. 15 and 16.

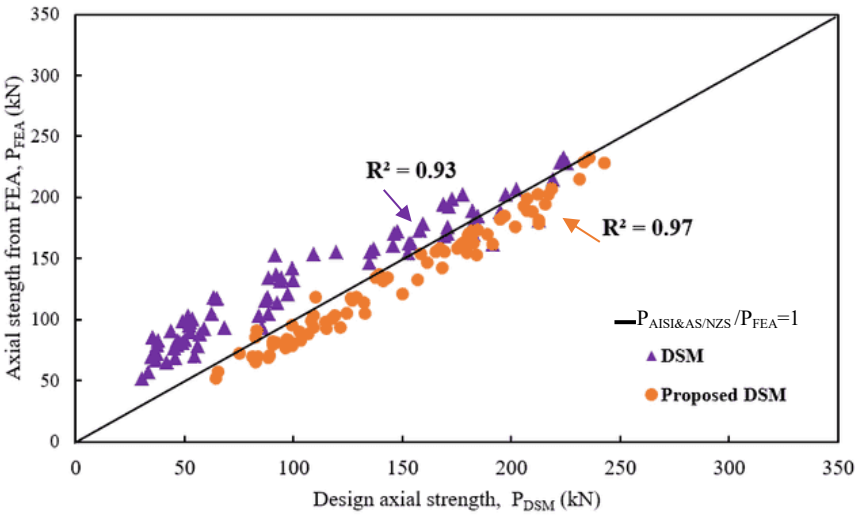

Fig. 15 Comparison of P_{FEA} versus P_{DSM} (2 mm)

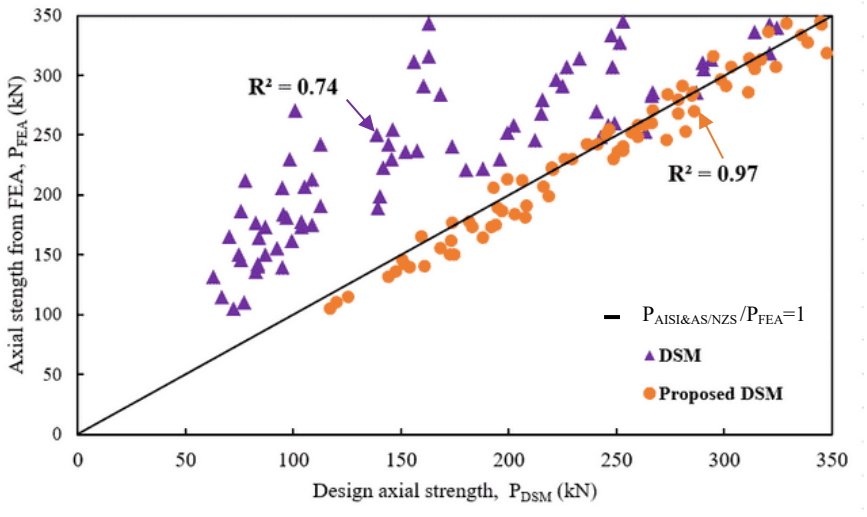

Fig. 16 Comparison of P_{FEA} versus P_{DSM} (3 mm)

7. Reliability analysis

The reliability of the proposed design equations was assessed using recommended design equations. According to the AISI S100-2016 [9] standard, a minimum reliability index (β) of 2.5 is advised for CFS members to ensure reliability. The reliability analysis conducted herein applied a load combination of 1.2 times Dead Load (DL) and 1.6 times Live Load (LL), following the American Society of Civil Engineers Standard (2005).

Statistical parameters such as the mean (P_m) and coefficient of variation (V_P) were determined for BBUAC120 and BBUAC150 sections with thicknesses of 2 mm and 3 mm, respectively. These parameters are critical for assessing the variability in material properties and loads.

Adjustment factors from the AISI S100-2016 [9] standard were used to calculate the reliability index. A resistance factor (φ=0.85) was consistently applied in the analysis. The results indicated that the proposed equations for predicting the axial capacity of both sections (BBUAC120 and BBUAC150) exceeded the minimum target reliability index (β) of 2.5. Therefore, the proposed design equations provide confidence in determining the concentric compressive strengths of BBUAC sections

8. Conclusion

This study investigated the concentric compressive strengths of CFS compound unequal angle section columns arranged back-to-back (BBUAC), both with and without stiffeners. The results of new experimental tests were presented, focusing on concentric compressive strengths, failure modes, and load versus axial displacement behavior. Nonlinear finite element analysis (FEA) models were developed and validated using these test results. A comprehensive parametric analysis involving 160 models was conducted to assess current design recommendations under the Direct Strength Method (DSM) against FE predictions.

Key conclusions drawn from this investigation include:

- Introducing a second intermittent stiffener in the longer leg of intermediate columns increased the strength of built-up sections by an average of 10%.
- Intermittent stiffeners in the shorter leg allowed for deflection along the major axis without significantly affecting concentric compressive strengths. These stiffeners enhanced the column's ability to resist major axis buckling by reducing plate slenderness.
- Stiffeners in the shorter leg effectively controlled major axis deflection but did not noticeably improve concentric compressive strengths.
- The strength of built-up columns decreased gradually with increasing length, primarily due to combined local and flexural buckling, leading to failure in columns longer than 600 mm.
- Current DSM methods tend to underestimate the concentric compressive strengths of BBUAC sections significantly. This study proposes refined design rules that consider both local and flexural buckling to better estimate these strengths.
- The proposed equations were validated through a comprehensive reliability analysis, ensuring accurate prediction of concentric compressive strengths for CFS angle sections with stiffeners.

These findings contribute to advancing the understanding and design methodologies for CFS compound unequal angle section columns, emphasizing the importance of intermittent stiffeners in enhancing structural performance against buckling while proposing improved design guidelines for practical applications.

Notations

A	Geometrical area;
A_e	Effective geometrical area;
CFS	Cold-formed steel;
AISI	American Iron and Steel Institute;
AS/NZS	Australian and New Zealand Standards;
DSM	Direct Strength Method;
EWM	Effective Width Method;
d_1	Longer leg dimension;
d_2	Shorter leg dimension;
d_3	Lip depth;
B	Total width = $2d_2$;
D	Total depth = d_1;
COV	Coefficient of variation;
FEM	Finite element modelling;
F_y	Yield strength;
F_n	Nominal compressive stress;
F_u	Ultimate tensile strength of steel;
f_y	Yield stress;
f_{ol}	Elastic local buckling stress;
f_{od}	Distortional buckling stress;
E	Modulus of elasticity;
L	Unbraced member length;
K	Effective length factor;
L_o	Gauge Length;
P_{DSM}	Design strength in accordance with AISI [5] & AS/NZS [6];
$P_{AISI/AS\&NZS}$	Compressive strength as per Direct Strength Method;
P_{EXP}	Axial capacity from the finite element analysis;
P_{FEA}	Axial capacity from experiments;
P_{cre}	Elastic flexural buckling load (critical);
T	Base metal thickness;
t	Thickness;
P_{nl}	Axial capacity for local buckling;
P_{nd}	Axial capacity for distortional buckling;
P_{ne}	Axial capacity for flexural buckling;
S	Spacing between the screws;
λ_l	Slenderness factor (local buckling);
λ_d	Slenderness factor (distortional buckling);
λ	Slenderness ratio;
DL	Dead load;
LL	Live load;

References

[1] Aruna G., Karthika V., Sukumar, S., "Finite element analysis and design of cold-formed steel built-up closed columns with flange and web intermediate stiffeners", *Canadian journal of civil engineering*, 47(10), 1175-1187, 2020. https://doi.org/10.1139/cjce-2019-0063.

[2] Ananthi G.B.G., Roy K., and Lim J.B.P, "Experimental and numerical investigations on axial strength of back-to-back built-up cold-formed steel angle columns", *Steel Compos. Struct., Int. J.*, 31(6), 601-615. 2019. https://doi.org/10.12989/scs.2019.31.6.601.

[3] Ananthi G.B.G., Roy K., Chen B., and Lim J.B.P., "Testing, simulation and design of back-to-back built-up cold-formed steel unequal angle sections under axial compression", *Steel Compos. Struct., Int. J.*, 33(4), 595-614. 2019. http://dx.doi.org/10.12989/scs.2019.33.4.595.

[4] Abdelrahman AH, Liu YP, Chan SL. Advanced joint slip model for single-angle bolted connections considering various effects. Advances in Structural Engineering. 2020 Jul;23(10):2121-2135.

[5] Abdelrahman AH, Du ZL, Liu YP, Chan SL. Stability design of single angle member using effective stress-strain method. Structures 2019 Aug 1 (Vol. 20, pp. 298-308).

[6] Hussain A, Liu YP, Chan SL. Finite element modeling and design of single angle member under bi-axial bending. Structures 2018 Nov 1 (Vol. 16, pp. 373-389). Elsevier.

[7] An LQ, Jiang WQ, Liu YP, Shi Q, Wang Y, Liu S. Experimental study of mechanical behavior of angles in transmission towers under freezing temperature. Advanced Steel Construction. 2018 Sep 1;14(3):461-78.

[8] Jiang WQ, Liu YP, Chan SL, Wang ZQ. Direct analysis of an ultrahigh-voltage lattice transmission tower considering joint effects. Journal of Structural Engineering. 2017 May 1;143(5):04017009.

[9] American Iron and Steel Institute, *North American specification for the design of cold-formed Steel Structural Members*; NAS S100. 2016.

[10] Standards Australia, "Cold-Formed Steel Structures", AS/NZS 4600:2018, *Standards Australia/ Standards New Zealand*. 2018.

[11] Ananthi G.B.G., Vishnuvardhan S and Knight G.M.S., "Experimental and numerical investigation on thin walled single and starred angle sections under compression", *Arabian Journal for Science and Engineering*, 40 (12), 3417-3427. https://doi.org/10.1007/s13369-015-1776-9. 2015.

[12] Ananthi G.B.G., Deepak M.S., Roy K., and Lim J.B.P., "Influence of intermediate stiffeners on the axial capacity of cold-formed steel back-to-back built-up unequal angle sections", *Structures.,* 32, 827-848. https://doi.org/10.1016/j.istruc.2021.03.059. 2021.

[13] Ananthi G.B.G., Roy K, Lim JB. Behaviour and strength of back-to-back built-up cold-formed steel unequal angle sections with intermediate stiffeners under axial compression. Steel and Composite Structures. 2022;42(1):1-22.

[14] Deepak MS, Ananthi G.B.G., Anupkumar GE, Harini BS, Kumar JM. Strength enhancements across various parts in intermediate and edge stiffened angle sections due to cold-forming. Materials Today: Proceedings. 2022 Jan 1; 65:1382-9.

[15] Vishnuvardhan S., "Behaviour of cold-formed steel single and compound angles in compression", Ph.D. Dissertation, Anna University, Chennai, India. 2006.

[16] Qu S., Zhang B., Guo Y., Sun Q., and Yi W., "Ultimate strength of pinned-end dual-angle cross combined section columns under axial compression", *Thin-Walled Structures*, 157, 107062. 2020. https://doi.org/10.1016/j.tws.2020.107062.

[17] Ananthi G.B.G., "A study on cold-formed steel compound angle section subjected to axial compression", *KSCE J. Civil Eng.*, 22(5), 1803-1815. https:// DOI 10.1007/s12205-017-1221-6. 2018.

[18] Dar M.A., Subramanian N., Rather A.I., Dar A.R., Lim J.B.P., Anbarasu M., and Roy K., "Effect of angle stiffeners on the flexural strength and stiffness of cold-formed steel beams", *Steel Compos. Struct., Int. J.*, 33(2), 225-243. 2019. https://doi.org/10.12989/scs.2019.33.2.225.

[19] El Aghoury M.A., El Salem A.H., Hanna M.T., and Amoush E.A, "Ultimate capacity of battened columns composed of four equal slender angles", *Thin-Walled Structures*, 63, 175-185. https://doi.org/10.1016/j.tws.2012.07.019. 2013.

[20] Anbarasu M., Adil, Dar M. "Improved design procedure for battened cold-formed steel built-up columns composed of lipped angles", *Journal of Constructional Steel Research*, 164, 105781. https://doi.org/10.1016/j.jcsr.2019.105781. 2020.

[21] Young B. and Chen J., "Column tests of cold-formed steel non-symmetric lipped angle sections", *J. Constr. Steel Res*., 64, 808-815. https://doi.org/10.1016/j.jcsr.2008.01.021. 2008.

[22] Shi G., Z. Liu, H.Y. Ban, Y. Zhang, Y.J. Shi, and Y.Q. Wang, "Tests and finite element analysis on the local buckling of 420 MPa steel equal angle columns under axial compression," *Steel Compos. Struct., Int. J*., 12(1), 31-51. https://doi.org/10.12989/scs.2011.12.1.031. 2011.

[23] Ellobody E. and Young B., "Design of cold-formed steel unequal angle compression members", *J. Constr. Steel Res.*, 45, 330-338. https://doi.org/10.1016/j.tws.2007.02.015. 2007.

[24] European Committee for Standardization (CEN), (2009), Metallic materials – Tensile testing. 1: method of test at room temperature', EN ISO 6892-1, Brussels, Belgium.

[25] ABAQUS (2018), Version 6.14-2, SIMULIA, Providence, RI, USA.

[26] Ananthi G.B.G., Roy K., Ghosh K, Pologanathan K, and Lim J.B.P, "An investigation on stiffened cold-formed steel unequal angle box section columns", *Journal of Building Engineering.*, 106989(76), 1-26. 2023. https://doi.org/10.1016/j.jobe.2023.106989.

[27] Fang Z., Roy K., Liang H., Pologanathan K., Ghosh K., Mohamed A.M., "Numerical simulation and design recommendations for web crippling strength of cold-formed steel channels with web holes under interior-one-flange loading at elevated temperatures", *Buildings,* 11 (12), 666. 2021.

[28] Fang Z., Roy K., Uzzaman A., Lim J.B.P., "Numerical simulation and proposed design rules of cold-formed stainless steel channels with web holes under interior-one-flange loading", *Engineering Structures,* 252, 113566. 2022.

[29] Roy K., Lau H.H., Ting T.C.H., Chen B., Lim J.B.P., "Flexural behaviour of back-to-back built-up cold-formed steel channel beams: Experiments and finite element modelling", *Structures,* 29, 235-253. 2021.

[30] Roy K, Lau HH, Lim JB. Finite element modelling of back-to-back built-up cold-formed stainless-steel lipped channels under axial compression. Steel Compos. Struct. 2019 Jan 1;33(1):37-66.

[31] Dai Y., Roy K., Fang Z., Chen B., Raftery G.M., Lim J.B.P., "A novel machine learning model to predict the moment capacity of cold-formed steel channel beams with edge-stiffened and un-stiffened web holes", *Journal of Building Engineering,* 53, 104592. 2022.

[32] Chen B, Roy K, Fang Z, Uzzaman A, Pham CH, Raftery GM, Lim JB. Shear capacity of cold-formed steel channels with edge-stiffened web holes, unstiffened web holes, and plain webs. Journal of Structural Engineering. 2022 Feb 1;148(2):04021268.

[33] Masood R., Lim J.B.P., VA González, K Roy, KIA Khan, "A systematic review on supply chain management in prefabricated house-building research", *Buildings* 12 (1), 40. 2022.

[34] Liang H, Roy K, Fang Z, Lim JB. A critical review on optimization of cold-formed steel members for better structural and thermal performances. Buildings. 2022, 12(1):34.

[35] Schafer, B.W. and Pekoz, T. (1998), "Computational modelling of cold-formed steel: characterizing Geometric imperfections and residual stress," J. Constr. Steel Res., 47, 193-210. https://doi.org/10.1016/S0143-974X (98)00007-8